Quantum Frontiers
上海交通大學 SHANGHAI JIAO TONG UNIVERSITY 李政道研究所 Tsung-Dao Lee Institute

ORIGINAL ARTICLE Open Access

Distant two-qubit gates in atomic array with Rydberg interaction using geometric quantum control

Ze-Rui He[1†], Zhao-Xin Fu[1†], Jia-Hao Liang[1], Zi-Yuan Chen[1], Hong-Zhi Liu[1], Jia-Yi Huang[1], Yue Ming[1], Zhi-Wei Han[1], Qing-Xian Lv[1], Yan-Xiong Du[1,2*] and Hui Yan[1,2*]

Abstract

Connectivity between qubits plays an irreplaceable role in quantum computation. An urgent task of quantum computation based on atomic arrays is to generate effective coupling between two distant qubits, thereby enhancing connectivity. In this paper, we investigate the realization of two-qubit gates utilizing buffer-atomic configuration, where the non-coding atoms serve as quantum buses to connect the computational qubits. Geometric control is achieved through globally-shined laser pulses in the Rydberg blockade region. It is found that acceleration based on shortcut to adiabaticity can be realized by reshaping the original control waveforms. The proposed distant two-qubit gate demonstrates robustness against systematic errors and random noise. Further numerical simulations indicate that high-fidelity control is maintained even when considering next-nearest-neighbor coupling among the atoms. Thus, our proposal provides a fast and experimentally feasible method for realizing distant two-qubit gates in atomic arrays, which may contribute to improving the scalability of quantum computations.

Keywords: Quantum computation, Atomic arrays, Geometric quantum control

1 Introduction

Atomic arrays in optical tweezers have emerged as promising physical platforms for large-scale quantum information processing [1–6]. These platforms have successfully demonstrated single-atom initialization, quantum gates, addressing, and readout. Two-qubit gates with neutral atoms are typically implemented by driving them to highly excited Rydberg states, which utilize strong and long-range interactions [7–9]. Over the past decade, significant advancements have been made to enhance gate fidelity, leading to the realization of two-qubit gates between neighboring atoms that surpass the quantum error-correction threshold [10–17]. It has been shown that quantum algorithms across N qubits demand a gate depth of $N^{1/D}$, where D is the dimension, assuming only nearest-neighbor couplings among qubits [18]. Quantum systems with high connectivity can perform quantum algorithms more efficiently than those with only local connections. Therefore, a crucial next step for single-atom platforms is the extension of two-qubit gates from neighboring to distant qubits [19, 20].

There are mainly two strategies to introduce effective interaction between two distant atoms. The first scheme is using optical or microwave photons as quantum buses to connect distant atoms [21–24]. However, these schemes

*Correspondence: yanxiongdu@m.scnu.edu.cn; yanhui@scnu.edu.cn
[1]Key Laboratory of Atomic and Subatomic Structure and Quantum Control (Ministry of Education), Guangdong Basic Research Center of Excellence for Structure and Fundamental Interactions of Matter, School of Physics, South China Normal University, Guangzhou 510006, China
[2]Guangdong Provincial Key Laboratory of Quantum Engineering and Quantum Materials, Guangdong-Hong Kong Joint Laboratory of Quantum Matter, Frontier Research Institute for Physics, South China Normal University, Guangzhou 510006, China
†Equal contributors

require precise experimental control of numerous parameters and must contend with photon loss in the cavity. The second strategy employs the so-called buffer-atom configuration, wherein non-encoding atoms in the array function as quantum buses. The Rydberg excitation of these buffer atoms can effectively couple computational qubits. This approach was proposed in [19], where the controlled-phase gates are realized by off-resonant coupling between ground states and Rydberg states to generate the appropriate phase shift [25–29]. The results are further generalized to accelerate the process by resonant coupling (between ground states and Rydberg states) via optimized algorithm [30]. Additionally, global laser pulses that simultaneously drive computational qubits and buffer atoms to implement distant two-qubit gates have been proposed [31]. However, adiabatic condition should be satisfied and the Rydberg interaction should switch its sign to realize the geometric control. Thus, further investigations are needed to achieve fast and robust control of distant two-qubit gates.

2 Physical model and the geometric manipulation

In the following, we describe the buffer-atomic configuration of N atoms employed for the realization of distant two-qubit gates. As illustrated in Fig. 1(a), two distant atoms, labeled by red points, are encoded as computational qubits. The blue points represent buffer atoms, which are used to induce effective coupling between the computational qubits via global excitation. The coupling strength between nearest-neighbor atoms is denoted by V_{NN}. Due to the $1/R^6$ scaling law of Rydberg interactions (R the distance between atoms), the coupling strength between next-nearest-neighbor atoms is significantly weaker than V_{NN}, yet it may still introduce unwanted effects. Since the linking patterns of buffer-atomic configuration may not be straight, the next nearest-neighboring couplings of the computational qubits-buffer atoms (as labelled by V_{NNN1}) and the buffer atoms-buffer atoms (as labelled by V_{NNN2}) maybe different.

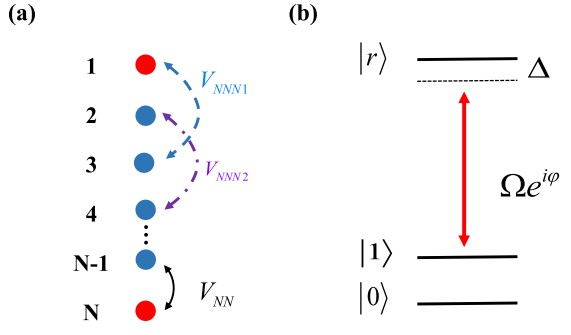

Figure 1 Illustration of quantum control with buffer-atomic configuration. (a) The buffer-atomic configuration of N atoms. Red points: computational qubits. Blue points: buffer atoms. Effective coupling between the computational qubits is achieved by exciting both the computational qubits and buffer atoms to Rydberg states. The coupling strength between nearest-neighboring atoms is denoted by V_{NN}. The next-nearest-neighbor coupling between the computational qubits and buffer atoms is labeled as V_{NNN1}, while the next-nearest-neighbor coupling among buffer atoms is labeled as V_{NNN2}. (b) The energy levels of the atoms. The states $|0\rangle$ and $|1\rangle$ are the ground states and $|r\rangle$ is the Rydberg state. The ground state $|1\rangle$ of each atom is coupled to the Rydberg state with Rabi frequency Ω, detuning Δ, and phase φ. At the beginning of the operation, all buffer atoms are prepared in the state $|1\rangle$, while the states of the computational qubits are arbitrary

As depicted in Fig. 1(b), each atom in Fig. 1(a) has three levels labeled by $|0\rangle, |1\rangle, |r\rangle$, where $|0\rangle$ and $|1\rangle$ are the ground states, and $|r\rangle$ is the Rydberg state. The ground state $|1\rangle$ of each atom is coupled to $|r\rangle$ with Rabi frequency Ω, detuning Δ, and phase φ. Initially, all buffer atoms are prepared in the state $|1\rangle$, while the states of the computational qubits are arbitrary. The total Hamiltonian of N interacting atoms is given by

$$H = \frac{\Omega}{2}\sum_k (\cos\varphi\sigma_x^k + \sin\varphi\sigma_y^k) + \Delta\sum_k n_k + \sum_{j,k} V_{j,k} n_j n_k, \tag{1}$$

where $\sigma_x^k = |1\rangle_k\langle r| + |r\rangle_k\langle 1|$, $\sigma_y^k = i(|1\rangle_k\langle r| - |r\rangle_k\langle 1|)$, $n_k = |r\rangle_k\langle r|$, and $\hbar = 1$. Here, $V_{j,k}$ represents the Rydberg interaction strength between the jth and kth atoms. It is well-established that a system governed by Hamiltonian (1) evolves within a Hilbert space of dimension 3^N. To further elucidate the features of the dynamics, we focus on the four computational basis: $|\widetilde{00}\rangle = |01\cdots10\rangle$, $|\widetilde{01}\rangle = |01\cdots11\rangle$, $|\widetilde{10}\rangle = |11\cdots10\rangle$, and $|\widetilde{11}\rangle = |11\cdots11\rangle$. Notably, an independent subspace associated with each computational basis state can be defined when the Rydberg blockade condition $V_{j,k} \gg \Omega, \Delta$ is satisfied.

For a system prepared in one of the basis states, it will evolve within the associated subspace. For example, in the case of $N = 3$ (one buffer atom), the four subspaces are constructed by $\{|\widetilde{00}\rangle, |0r0\rangle\}$, $\{|\widetilde{01}\rangle, |0r1\rangle, |01r\rangle\}$, $\{|\widetilde{10}\rangle, |1r0\rangle, |r10\rangle\}$, and $\{|\widetilde{11}\rangle, |\tilde{r}_1^1\rangle, |\tilde{r}_1^2\rangle, |\tilde{r}_1^3\rangle, |\tilde{r}_2\rangle\}$. Here, $|\tilde{r}_1^1\rangle = |r11\rangle$, $|\tilde{r}_1^2\rangle = |1r1\rangle$, and $|\tilde{r}_1^3\rangle = |11r\rangle$ represent the single Rydberg excitation states, while $|\tilde{r}_2\rangle = |r1r\rangle$ represents the dual Rydberg excitation state (simultaneous excitation of two neighboring atoms is forbidden due to the Rydberg blockade condition). The Hamiltonian for each subspace is computed by $H_s^{jk} = \langle j|H|k\rangle$, where $|j(k)\rangle$ are the basis of the corresponding subspace $s = \widetilde{00}, \widetilde{01}, \widetilde{10}, \widetilde{11}$, and we obtain

$$H_{\widetilde{00}} = (\frac{\Omega}{2}e^{i\varphi}|\widetilde{00}\rangle\langle 0r0| + \mathrm{H.c.}) + \Delta|0r0\rangle\langle 0r0|, \tag{2a}$$

$$H_{\widetilde{01}} = (\frac{\Omega}{2}e^{i\varphi}|\widetilde{01}\rangle\langle 01r| + \frac{\Omega}{2}e^{i\varphi}|\widetilde{01}\rangle\langle 0r1| + \mathrm{H.c.}) + \Delta(|0r1\rangle\langle 0r1| + |01r\rangle\langle 01r|), \tag{2b}$$

$$H_{\widetilde{10}} = (\frac{\Omega}{2}e^{i\varphi}|\widetilde{10}\rangle\langle 1r0| + \frac{\Omega}{2}e^{i\varphi}|\widetilde{10}\rangle\langle r10| + \text{H.c.}) + \Delta(|r10\rangle\langle r10| + |1r0\rangle\langle 1r0|), \tag{2c}$$

$$H_{\widetilde{11}} = (\frac{\sqrt{3}\Omega}{2}e^{i\varphi}|\widetilde{11}\rangle\langle R_3| + \frac{\sqrt{2}\Omega}{2}e^{i\varphi}|\tilde{r}_2\rangle\langle R_2| + \text{H.c.}) + \Delta(\sum_k |\tilde{r}_1^k\rangle\langle\tilde{r}_1^k| + 2|\tilde{r}_2\rangle\langle\tilde{r}_2|), \tag{2d}$$

where $|R_3\rangle = \sum_k |\tilde{r}_1^k\rangle/\sqrt{3}$, $|R_2\rangle = (\tilde{r}_1^1 + \tilde{r}_1^3)/\sqrt{2}$. The Hamiltonian of subspace can be parameterized by $H_s = H_s(\theta, \varphi)$ and $\tan\theta = \Omega/\Delta$. We adopt the orange-slice model to drive the system of which of the control parameters of Hamiltonian (1) are given by:

$$\Omega = \Omega_0 \sin(\pi t/T), \Delta = \Omega_0 \cos(\pi t/T), \varphi = 0, \tag{3}$$

for $t : 0 \to T$, T is the evolution period.

$$\Omega = \Omega_0 \sin(\pi(t-T)/T), \Delta = \Omega_0 \cos(\pi(t-T)/T), \varphi = \Delta\varphi, \tag{4}$$

for $t : T \to 2T$. Since the energy gaps of each subspace are proportional to $\Omega_0 = \sqrt{\Omega^2 + \Delta^2}$, the condition $\Omega_0 T \gg \pi$ is sufficient to ensure adiabatic evolution. For a system prepared in each computational basis $|\Psi_s\rangle = \{|\widetilde{00}\rangle, |\widetilde{01}\rangle, |\widetilde{10}\rangle, |\widetilde{11}\rangle\}$, it will evolve along the lowest eigenstate of the Hamiltonian H_s, as $|\Psi_s\rangle$ is the lowest energy states and θ starts from 0 according to the control scheme. It can be verified that θ evolves along $0 \to \pi \to 0$. The computational basis $|\Psi_s\rangle$ will evolve along a closed path in the Hilbert space to gain the geometric phase given by $\gamma_g^s = \int_0^{2T} i\langle\Psi_s|\partial_t|\Psi_s\rangle$. The dynamical phases of $|\Psi_s\rangle$ are canceled due to the time-reversal operations of Eqs. (3) and (4) of which the dynamical phases are $\gamma_d^{s1} = \int_0^{2T} i\langle\Psi_s|H_s|\Psi_s\rangle$ and $\gamma_d^{s2} = -\gamma_d^{s1}$, respectively [32–41]. For N-atom system in Fig. 1(a) prepared in the state $|\Psi_0\rangle = \sum_k a_k|\Psi_s\rangle$, the final state after the geometric control will be $|\Psi_f\rangle = \sum_k a_k e^{i\gamma_k}|\Psi_s\rangle$, where $k = 1, 2, 3, 4$ denote the case of $\widetilde{00}$, $\widetilde{01}$, $\widetilde{10}$, and $\widetilde{11}$, respectively. Therefore, by carefully designing the control parameters, a $\delta\gamma$ controlled-phase gate can be achieved with $\delta\gamma = \gamma_1 + \gamma_2 + \gamma_3 - \gamma_4$.

In the following, we investigate the acceleration of adiabatic control for Hamiltonian (1), as long control times required by the adiabatic condition can lead to reduced fidelity due to decoherence. According to the shortcut to adiabaticity theory for non-degenerate states, the auxiliary terms that cancel the diabatic effects are given by $H_s^a = i\sum\left(|\partial_t\lambda_k^s\rangle\langle\lambda_k^s| - \langle\lambda_k^s|\partial t\lambda_k^s\rangle|\lambda_k^s\rangle\langle\lambda_k^s|\right)$, where λ_k^s is the eigenstate of subspace s [42–47]. We consider the case of $N = 3$. When $s = \widetilde{00}, \widetilde{01}$, and $\widetilde{10}$, $H_s^a = i\Omega_a/2e^{i\varphi}|\Psi_s\rangle\langle r_s| + \text{H.c.}$, $\Omega_a = \dot{\theta}$ as computed by the eigenstates of H_s. Here, $|r_{\widetilde{00}}\rangle = |0r0\rangle$, $|r_{\widetilde{01}}\rangle = |01r\rangle$, and $|r_{\widetilde{10}}\rangle = |1r0\rangle$. When $s = \widetilde{11}$, the auxiliary Hamiltonian will be more complicated and different from the other cases. Since the four subspaces s are embedded in the same Hamiltonian (1) and are manipulated synchronously, we adopt Ω_a as the auxiliary Rabi frequency. The modified control waveform for Hamiltonian (1) is given by $\Omega_{\text{m}} = \sqrt{\Omega^2 + \Omega_a^2}$, $\Delta_{\text{m}} = \Delta$, and $\varphi_{\text{m}} = \varphi + \arctan\Omega_a/\Omega$. The modified waveforms used for geometric control are shown in Fig. 2(a). Here, we set $\Omega_0 = 2\pi \times 10$ MHz, $T = 250$ ns, and $\delta\varphi = \pi/2$.

For the system prepared in the computational basis $\widetilde{00}$, $\widetilde{01}$ ($\widetilde{10}$), and $\widetilde{11}$, the dynamics is shown in Fig. 2(b), 2(c), and 2(d), respectively. The black-dashed lines represent the population P_k, while the red-solid lines correspond to the accumulating phases γ_k. As can be observed, the populations return to their initial values after the geometric control. The additional acquired phases are $\gamma_1 = \gamma_2 = \gamma_3 = -\pi/2$ and $\gamma_4 = -\pi$, resulting in a phase difference of $\Delta\gamma = -\pi/2$, as indicated by the results in Fig. 2. Consequently, a geometric $-\pi/2$ controlled-phase gate between distant qubits using buffer atoms can be achieved.

3 Robustness of the distant two-qubit gate

In Fig. 3, the acceleration of the modified pulses shown in Fig. 2(a) is investigated for $N = 3$. The initial state is set to $|\Psi_{\text{i}}\rangle = (|\widetilde{00}\rangle + |\widetilde{01}\rangle + |\widetilde{10}\rangle + |\widetilde{11}\rangle)/2$ to ensure generality. The final state of the controlled-phase gate, after the manipulation of the modified or adiabatic pulses, is denoted as $|\Psi_{\text{f}}\rangle$. The dynamics are computed by the Schrödinger Equation with the complete Hamiltonian given by Eq. (1). The parameters are set to $T = 250$ ns and ΩT change from 4π to 16π. The Rydberg interaction strength is chosen as $V_{j,j+1} = V = 2\pi \times 400$ MHz to satisfy the Rydberg blockade condition, with $V_{j,k} = 0$ for $|j-k| > 1$. The fidelity is derived by $F = |\langle\Psi_{\text{cp}}|\Psi_{\text{f}}\rangle|^2$, where $|\Psi_{\text{cp}}\rangle$ represents the ideal state after the controlled-phase gate. It is evident that the fidelity F of the modified pulse (red-dashed line) is more robust than that of the adiabatic pulse (black-solid line). Due to the non-synchronous dynamics of the computational basis, the diabatic effect is not perfectly canceled, leading to a slight drop in the fidelity of the modified pulse as ΩT decreases. However, the fidelity of the modified pulse is above 0.995 for $\Omega T > 10\pi$, which is sufficiently high for quantum computation.

Figure 4(a) illustrates the robustness of distant controlled-phase gate against the variations of Rabi frequencies. These variations typically arise from the thermal motion of atoms due to the tight focusing of the Rydberg excitation lasers on the atoms. The initial state $|\Psi_{\text{i}}\rangle$ is the same with Fig. 3 (as also as Fig. 4(b) and 4(c)). Here, we rewrite the Rabi frequencies by $\Omega' = \Omega_0(1 + \eta_\Omega)$, $\eta_\Omega \in [-0.1, 0.1]$. As shown in Fig. 4(a), the fidelities of $N = 3$ (red-solid line) and $N = 4$ (black-dashed line) atoms are higher than 0.995 and robust against variations of Ω in the range of ± 0.1. As the number of buffer atoms increases, more eigenstates become involved in the dynamics, leading to greater leakage to the outside space. The increase of

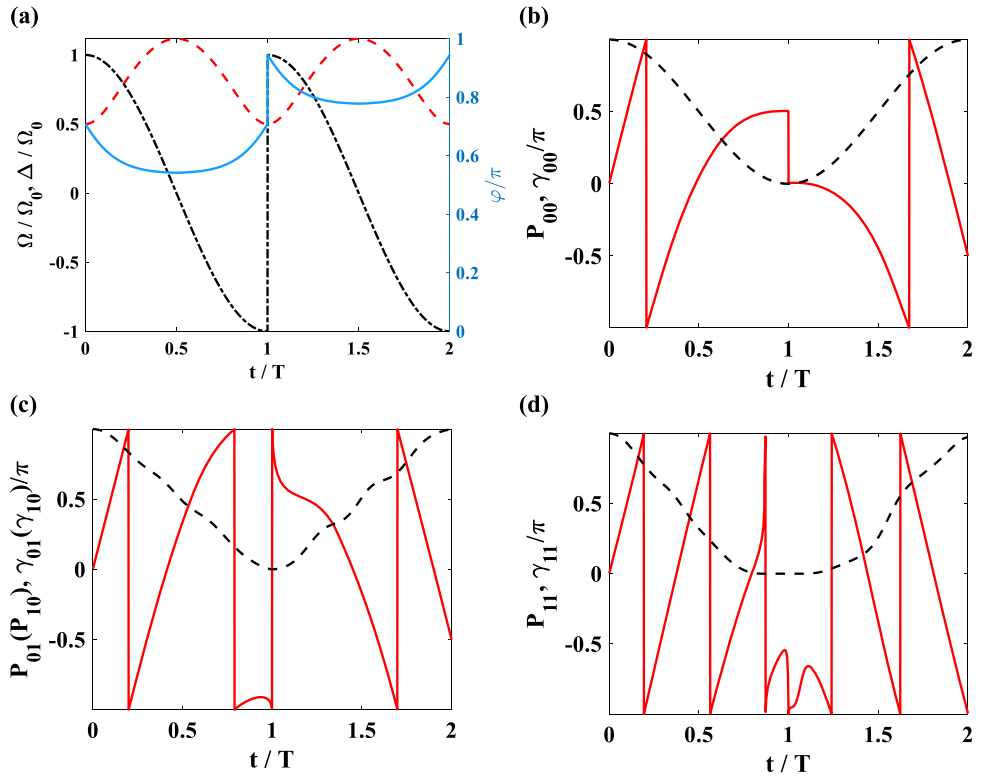

Figure 2 Geometric control of two distant qubits under the Rydberg blockade condition. (a) Control waveforms. Time-reversal operations are adopted to cancel the dynamical phases and shortcut to adiabatic theory is used to accelerate the adiabatic control. Red-dashed line: Rabi frequency. Black dashed-dotted line: detuning. Blue-solid line: phase. (b), (c), (d) The dynamics of the computational basis $|\widetilde{00}\rangle, |\widetilde{01}\rangle, |\widetilde{10}\rangle, |\widetilde{11}\rangle$ for $N = 3$ atoms under the driving of Hamiltonian (2a) to (2d). Black-dashed lines: population. Red-solid lines: the accumulating phases. The parameters are chosen to be $\Omega_0 = 2\pi \times 10$ MHz, $T = 250$ ns, and $\Delta\varphi = \pi/2$. According to the simulation results, a geometric $-\pi/2$ controlled-phase gate between distant qubits is achieved

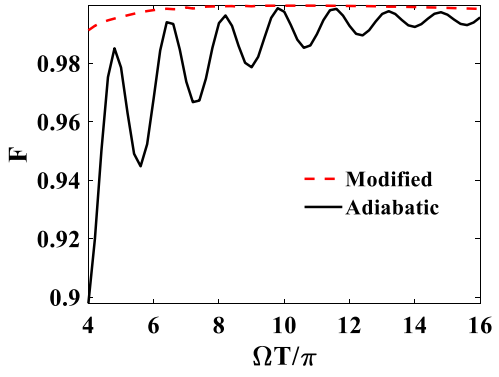

Figure 3 Fidelity F of distant two-qubit gate versus different ΩT. Here, $N = 3$ buffer-atomic configuration is adopted. Black-solid line: adiabatic control using Eq. (3) and (4). Red-dashed line: modified pulse using waveforms in Fig. 2(a). The initial state is set to be $|\Psi_i\rangle = (|\widetilde{00}\rangle + |\widetilde{01}\rangle + |\widetilde{10}\rangle + |\widetilde{11}\rangle)/2$. It is evident that geometric control based on the modified pulse is more robust against variations of ΩT

Rabi frequencies results higher fidelity by relaxing the adiabatic condition, and thus, for $N = 5$ (blue dashed-dotted line), the fidelity ramps slightly as Ω' increases. In Fig. 4(b), the robustness of the proposed gate against random noise of the Rabi frequencies is investigated. The random noise of Rabi frequencies is introduced by $\Omega'' = \Omega_0(1 + \eta_\Omega^r)$, η_Ω^r are random numbers in the region $[-0.1, 0.1]$ with zero mean values. The fidelities F of $N = 3, 4, 5$ are robust against the fluctuation of Rabi frequencies since the fluctuation does not affect the cancellation of the dynamics phase. In Fig. 4(c), the robustness of the proposed gate against random noise of the detuning is investigated where the actual detuning are replaced by $\Delta'' = \Omega_0(1 + \eta_\Delta^r)$, η_Δ^r are random numbers in the region $[-0.1, 0.1]$ with zero mean values. The fidelities F of $N = 3, 4, 5$ are all higher than 0.99 in the range of $[-0.05, 0.05]$ since the proposed gate utilizes the geometric phases. Note that the data of the case of random niose have been averaged for 100 times. The proposed gate is also robust against the deviation of detuning. In actual experiments, the detuning can be controlled accurately and the inhomogeneity of detuning is small. Thus,

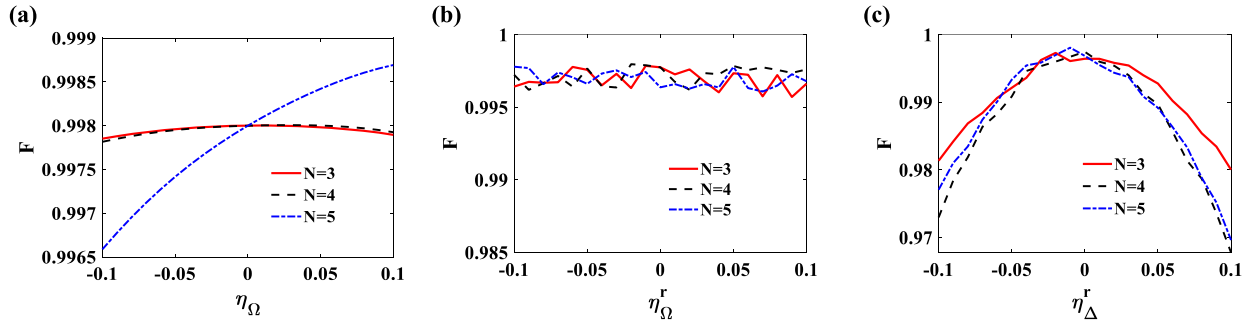

Figure 4 Robustness of distant two-qubit gate with geometric control. (a) Fidelity F versus the variation of the Rabi frequency Ω. (b) Fidelity F versus the random noise in the Rabi frequency Ω. (c) Fidelity F versus the random noise in the detuning Δ. Red-solid lines: $N = 3$ buffer-atomic configurations. Black-dashed lines: $N = 4$. Blue dashed-dotted lines: $N = 5$

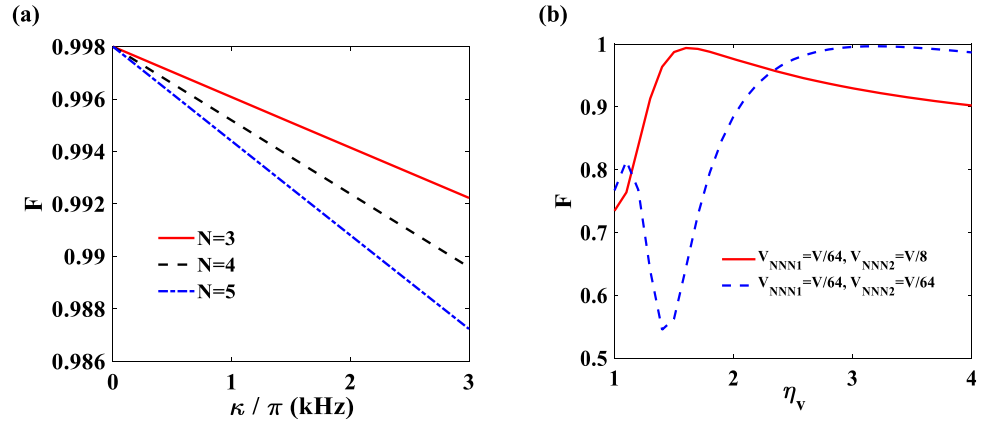

Figure 5 (a) Fidelity F of distant two-qubit gate versus different decay rate κ of Rydberg state. Red-solid lines: $N = 3$ buffer-atomic configuration. Black-dashed lines: $N = 4$. Blue dashed-dotted lines: $N = 5$. (b) The effect of finite next nearest-neighboring coupling upon fidelity F of distant two-qubit gate. In the line-shape configuration, $V_{\mathrm{NNN1}} = V_{\mathrm{NNN2}}$ while in th Z-shape $V_{\mathrm{NNN1}} \neq V_{\mathrm{NNN2}}$. There are optimal Rydberg interaction strength after considering the next nearest-neighboring coupling

the distant two-qubit gate based on buffer atoms with geometric control demonstrates robustness against both systematic errors and random noise.

The effect of decoherence on the proposed gate is analyzed in Fig. 5(a). We primarily consider the decay from the Rydberg states of which is introduced by $\Delta' = \Delta + i\kappa$, and the dynamics are obtained by solving the Schrödinger Equation. The control parameters and initial state are the same as those in Fig. 3. For the case of $N = 3$ (red-solid line), the fidelity F is higher than 0.995 when $\kappa < 2\pi \times 1$ kHz [48]. As more buffer atoms are included, the fidelities become increasingly sensitive to the decay rate, with the black-dashed line representing the result for $N = 4$, and the blue dash-dotted line for $N = 5$. As a consequence, the decay rate of the Rydberg states emerges as a primary limitation for the scalability of buffer-atom mediated quantum computation. It matters that the potential scalability of the system after considering the decay. The infidelity of the proposed gate for N atoms can be estimated as $F_{\mathrm{infd}} = \frac{7\pi}{4\Omega\tau}(1 + \frac{\Omega^2}{\omega_{10}^2} + \frac{(N-1)^2\Omega^2}{7V_d^2}) + \frac{(N-1)^2\Omega^2}{8V_d^2}(1 + 6\frac{V_d^2}{\omega_{10}^2})$, where τ is the lifetime of the Rydberg state, ω_{10} is the energy splitting between $|1\rangle$ and $|0\rangle$, and V_d is the Rydberg interaction strength [1]. Considering the Rydberg state $|n = 79\rangle$ of Rb_{87} with 2 μm atom spacing, $\omega_{10} = 6.8$ GHz, $\tau = 200\mu s$ [48], and $V_d = 36$ GHz. By setting $\Omega = 0.05$ GHz [17], one finds that the maximum number N to achieve $F_{\mathrm{infd}} < 0.05$ will be $N = 10$.

In Fig. 5(b), the effect of next-nearest-neighbor coupling is considered. Due to the $1/R^6$ scaling law (R is the distance between two atoms), the strength of the next-nearest-neighbor coupling is 1/64 that of the nearest-neighbor coupling when the distance between atoms is doubled. There are primarily two types of linking patterns for buffer atom configurations in two-dimensional square arrays: the line-shaped configuration (where the connecting lines be-

tween computational qubits and buffer atoms are parallel to the inter-chain of buffer atoms) and the Z-shaped configuration (where the connecting lines are perpendicular to the inter-chain of buffer atoms). In the case of the line-shaped configuration, $V_{\mathrm{NNN1}} = V_{\mathrm{NNN2}} = V/64$, V is the nearest-neighbor coupling strength between two atoms, V_{NNN1} is the next-nearest-neighbor coupling strength between the computational qubit and the buffer atoms, and V_{NNN2} is the next-nearest-neighbor coupling strength between two buffer atoms. For the Z-shaped configuration, $V_{\mathrm{NNN1}} = V/8$ and $V_{\mathrm{NNN2}} = V/64$. In the simulation shown in Fig. 5(b), the initial state $|\Psi_{\mathrm{i}}\rangle$ is the same as in Fig. 3. The system is operated with the pulses in Fig. 2(a). The parameters are set as $\Omega = 2\pi \times 1$ MHz, $\Omega T = 10\pi$, and the nearest-neighbor coupling strength is $V = \eta_v V_0$, with $V_0 = 2\pi \times 100$ MHz. The fidelities of the distant controlled-phase gate are shown in Fig. 5(b): the red-solid line represents the Z-shaped configuration, and the blue-dashed line represents the line-shaped configuration. Decoherence is not considered in this simulation. As can be seen, after considering the next nearest-neighbouring coupling, the Rydberg interaction strength V must be 100 times larger than the Rabi frequencies Ω. There is an optimal value of V where the ratio η_v for the Z-shaped configuration is smaller, while the line-shaped configuration exhibits greater robustness against variations in V near the optimal value. These results suggest that further optimization of the buffer-atomic configuration could enhance robustness and reduce the required interaction strength.

4 Discussions

In the following, we discuss the influence of the relative phases of buffer atoms, the acceleration of modified pulses, and the comparison between the buffer-atom configuration and other schemes.

To consider the influence of the relative phases of the buffer atoms, the computational basis of the N atoms can be rewritten as $|\Psi'_{\widetilde{jk}}\rangle = |j\rangle \otimes |b_1\rangle \otimes |b_2\rangle \otimes \cdots \otimes |b_{N-2}\rangle \otimes |k\rangle$, $j, k = 0, 1$, and $|b_m\rangle = |1_m\rangle e^{i\phi_m}$, b_m is the mth buffer atom. One can find that $|\Psi'_{\widetilde{jk}}\rangle = |\Psi_{\widetilde{jk}}\rangle e^{i\sum_m \phi_m}$, the summation is over the numbers of buffer atoms. Therefore, the relative phases of the buffer atoms only bring a global phase to the computational basis $|\Psi_{\widetilde{jk}}\rangle$. In our proposed scheme, the population of buffer atoms is driven from the initial state $|1\rangle$ and returns to the same state. The buffer-atomic configuration remains reusable, provided that the control fidelity is sufficiently high.

In the discussion of Sect. 2, modified pulses are put forward to accelerate the dynamics. We cancel the diabatic effect through shortcut to adiabatic theory, yet the formulation is incomplete because of the asynchronous dynamics of the four subspaces. To fully address this issue, one could derive the eigenstates of Hamiltonian (1) to compute the auxiliary Hamiltonian H_a, which is a challenging task for many-body systems. Experimental challenges also arise since the form of H_a is likely to be complex and difficult to realize experimentally. A compromising strategy is to use the parallel adiabatic passage. The adiabatic condition can be characterized by $\beta = \dot{\theta}/\Delta\lambda_{\mathrm{min}}$, $\beta \ll 1$. $\Delta\lambda_{\mathrm{min}}$ is the minimal energy gap between the ground state and the first excited state, which is proportional to $\Omega/(V - \Delta) + \Omega/(2V - \Delta)$ [31]. Therefore, given certain values of θ, β, and V, we will derive Ω_0 and thus the protocol can be determined.

It may also be essential to compare the quantum control based on buffer-atom configuration with existing methods, for example, the distant connection by coherently transporting atoms [49] and cavity-mediated interactions [50]. The success possibility of transporting atoms will be the vital limitation of the transporting atom scheme. In typical experiments [49], the success possibility of transporting atoms S_{t} decreases linearly with a relationship $S_{\mathrm{t}} = 1 - 0.004N$ with short distance, N are the separation numbers. The success possibility of a forward-backward control will be given by S_{t}^2 and smaller than 0.97 when $N > 4$. The main limitation of promoting S_{t} is the background vacuum. To raise the S_{t}, a science chamber with high vacuum is needed [51]. An intelligent experiment shows that atoms can be manipulated within optical cavity. Entanglement is generated with 6 atoms at most. The generation probability exceeds 97%, and the fidelity is over 87%, and the limitation is due to the overall transmission and detection efficiency. The scaling of atom numbers is restricted to the finite cavity mode size.

Finally, we compare the connectivity of atomic arrays based on buffer-atomic configurations with the trapped ion systems that rely on phonon-mediated gates. The essential two-qubit logic gate in trapped ion systems based on single-mode phonon is typically performed in an adiabatic regime. This results in slower two-qubit gate speeds compared to the characteristic motional frequencies of the ions in the trap, which are on the order of 10 kHz [52, 53]. Additionally, the single-mode approach is difficult to scale because isolating individual modes becomes increasingly challenging as the number of ions grows. Multi-mode schemes are scalable but limited to pairwise gates. As shown in Figs. 5(a) and 5(b), a distant two-qubit gate with high fidelity for $N = 5$ atoms can be achieved based on the experimental parameters. The gate speed exceeds 100 kHz. Further improvements, such as increasing the Rydberg interaction strength, reducing the decay rate of Rydberg states, and optimizing buffer-atom configurations, can extend the distance between computational qubits. Therefore, the distant two-qubit gate based on geometric control presents an effective approach for realizing large-scale quantum computation.

5 Conclusion

In summary, we have introduced a new protocol for the realization of controlled-phase gates upon two distant

qubits, using the buffer-atom configuration in atomic arrays. Geometric control is achieved through global-shinning laser pulses, with parameters satisfying the Rydberg blockade condition. It is found that acceleration can be achieved by reshaping the original control waveforms, which is experimentally friendly. The proposed distant two-qubit gate is shown to be robust against systematic errors and random noise. Further numerical simulations demonstrate that high-fidelity control can still be maintained, even when accounting for next-nearest-neighbor coupling of the atoms. Therefore, our proposal provides a fast and experimentally viable approach to realize distant two-qubit gates in atomic arrays with analytical control waveforms.

Acknowledgements
The authors thank Yuan Sun for helpful discussions.

Author contributions
YD and HY proposed the idea and supervised the project. ZRH and ZF contributed equally to this work. ZRH, ZF and YD carried out the calculations. JL, ZC, HL, JH, YM and ZWH analyzed the data, discussed the results. YD, QL and HY wrote the manuscript. All authors read and approved the final manuscript.

Funding
This work was supported by the National Natural Science Foundation of China (Grants No. 12225405, No. U20A2074, No. 12304287, No. 12074180, No. 12074132 and No. 12304287), the Innovation Program for Quantum Science and Technology (Grant No. 2021ZD0301700), the National Key Research and Development Program of China (Grant No. 2022YFA1405300), the Project funded by China Postdoctoral Science Foundation (Grant No. 2022M721222, No. 2023T160233), Guangdong Basic and Applied Basic Research Foundation (Grants No. 2023A1515011550 and No. 2024A1515012516) and Guangdong Provincial Quantum Science Strategic Initiative (Grant No. GDZX2304002, No. GDZX2303006).

Data availability
All data underlying the results are available from the corresponding authors upon reasonable request.

Declarations

Competing interests
The authors declare no competing interests.

Received: 17 September 2024 Revised: 3 November 2024
Accepted: 7 November 2024 Published online: 03 December 2024

References

1. Saffman M, Walker TG, Mølmer K (2010) Quantum information with Rydberg atoms. Rev Mod Phys 82:2313–2363
2. Saffman M (2016) Quantum computing with atomic qubits and Rydberg interactions: progress and challenges. J Phys B, At Mol Opt Phys 49:202001
3. Henriet L, Beguin L, Signoles A, Lahaye T, Browaeys A, Reymond GO, Jurczak C (2020) Quantum computing with neutral atoms. Quantum 4:327
4. Browaeys A, Lahaye T (2020) Many-body physics with individually controlled Rydberg atoms. Nat Phys 16:132–142
5. Scholl P, Schuler M, Williams HJ, Eberharter AA, Barredo D, Schymik KN, Lienhard V, Henry LP, Lang TC, Lahaye T, Läuchli AM, Browaeys A (2021) Quantum simulation of 2D antiferromagnets with hundreds of Rydberg atoms. Nature 595:233–238
6. Ebadi S, Wang TT, Levine H, Keesling A, Semeghini G, Omran A, Bluvstein D, Samajdar R, Pichler H, Ho WW, Choi S, Sachdev S, Greiner M, Vuletić V, Lukin MD (2021) Quantum phases of matter on a 256-atom programmable quantum simulator. Nature 595:227–232
7. Jaksch D, Cirac JI, Zoller P, Rolston SL, Côté R, Lukin MD (2000) Fast quantum gates for neutral atoms. Phys Rev Lett 85:2208–2211
8. Saffman M, Walker TG (2005) Analysis of a quantum logic device based on dipole-dipole interactions of optically trapped Rydberg atoms. Phys Rev A 72:022347
9. Senhower L, Saffman M, Mølmer K (2011) Multibit C_kNOT quantum gates via Rydberg blockade. Quantum Inf Process 10:755–770
10. Maller KM, Lichtman MT, Xia T, Sun Y, Piotrowicz MJ, Carr AW, Isenhower L, Saffman M (2015) Rydberg-blockade controlled-not gate and entanglement in a two-dimensional array of neutral-atom qubits. Phys Rev A 92:022336
11. Jau YY, Hankin AM, Keating T, Deutsch IH, Biedermann GW (2016) Entangling atomic spins with a Rydberg-dressed spin-flip blockade. Nat Phys 12:71–74
12. Levine H, Keesling A, Omran A, Bernien H, Schwartz S, Zibrov AS, Endres M, Greiner M, Vuletić V, Lukin MD (2018) High-fidelity control and entanglement of Rydberg-atom qubits. Phys Rev Lett 121:123603
13. De Léséleuc S, Barredo D, Lienhard V, Browaeys A, Lahaye T (2018) Analysis of imperfections in the coherent optical excitation of single atoms to Rydberg states. Phys Rev A 97:053803
14. Liu YY, Fu Z, Xu P, He XD, Wang J, Zhan MS (2021) Spectral filtering of dual lasers with a high-finesse length-tunable cavity for rubidium atom Rydberg excitation. Chin Phys B 30:074203
15. Madjarov IS, Covey JP, Shaw AL, Choi J, Kale A, Cooper A, Pichler H, Schkolnik V, Williams JR, Endres M (2020) High-fidelity entanglement and detection of alkaline-Earth Rydberg atoms. Nat Phys 16:857–861
16. Zeng Y, Xu P, He X, Liu Y, Liu M, Wang J, Papoular DJ, Shlyapnikov GV, Zhan MS (2017) Entangling two individual atoms of different isotopes via Rydberg blockade. Phys Rev Lett 119:160502
17. Evered SJ, Bluvstein D, Kalinowski M, Ebadi S, Manovitz T, Zhou H, Li SH, Geim AA, Wang TT, Maskara N, Levine H, Semeghini G, Greiner M, Vuletić V, Lukin MD (2023) High-fidelity parallel entangling gates on a neutral-atom quantum computer. Nature 622:268–272
18. Boixo S, Isakov SV, Smelyanskiy VN, Babbush R, Ding N, Jiang Z, Bremner MJ, Martinis JM, Neven H (2018) Characterizing quantum supremacy in near-term devices. Nat Phys 14:595
19. Sun Y (2024) Buffer-atom-mediated quantum logic gates with off-resonant modulated driving. SCPMA. https://doi.org/10.1007/s11433-024-2478-8
20. Ramette J, Sinclair J, Vendeiro Z, Rudelis A, Cetina M, Vuletić V (2022) Any-to-any connected cavity-mediated architecture for quantum computing with trapped ions or Rydberg arrays. PRX Quantum 3:010344
21. Sárkány L, Fortágh J, Petrosyan D (2015) Long-range quantum gate via Rydberg states of atoms in a thermal microwave cavity. Phys Rev A 92:030303
22. Sárkány L, Fortágh J, Petrosyan D (2018) Faithful state transfer between two-level systems via an actively cooled finite-temperature cavity. Phys Rev A 97:032341
23. Kaiser M, Glaser C, Ley LY, Grimmel J, Hattermann H, Bothner D, Koelle D, Kleiner R, Petrosyan D, Günther A, Fortágh J (2022) Cavity-driven Rabi oscillations between Rydberg states of atoms trapped on a superconducting atom chip. Phys Rev Res 4:013207
24. Ocola PL, Dimitrova I, Grinkemeyer B, Guardado-Sanchez E, Dordevic T, Samutpraphoot P, Vuletić V, Lukin MD (2024) Control and entanglement of individual Rydberg atoms near a nanoscale device. Phys Rev Lett 132:113601
25. Sun Y, Xu P, Chen PX, Liu L (2020) Controlled phase gate protocol for neutral atoms via off-resonant modulated driving. Phys Rev Appl 13:024059
26. Sun Y (2023) Off-resonant modulated driving gate protocols for two-photon ground-Rydberg transition and finite Rydberg blockade strength. Opt Express 31:3114–3121
27. Li XX, Shao XQ, Li WB (2022) Single temporal-pulse-modulated parameterized controlled-phase gate for Rydberg atoms. Phys Rev Appl 18:044042
28. Fu Z, Xu P, Sun Y, Liu YY, He XD, Li X, Liu M, Li RB, Wang J, Liu L, Zhan MS (2022) High-fidelity entanglement of neutral atoms via a Rydberg-mediated single-modulated-pulse controlled-phase gate. Phys Rev A 105:042430
29. Chen ZY, Liang JH, Fu ZX, Liu HZ, He ZR, Wang M, Han ZW, Huang J-Y, Lv QX, Du YX (2024) Single-pulse two-qubit gates for Rydberg atoms with noncyclic geometric control. Phys Rev A 109:042621

30. Fan XY, Wang X, Sun Y (2024) Fast entangling quantum gates with almost-resonant modulated driving. Fund Res. https://doi.org/10.1016/j.fmre.2024.07.002
31. Doultsinos G, Petrosyan D (2024) Quantum gates between distant atoms mediated by a Rydberg excitation antiferromagnet. arXiv:2408.11542
32. Berry MV (1984) Quantal phase factors accompanying adiabatic changes. Proc R Soc Lond A 392:45–57
33. Duan LM, Cirac JI, Zoller P (2001) Geometric manipulation of trapped ions for quantum computation. Science 292:1695–1697
34. Zhu SL, Wang ZD (2003) Unconventional geometric quantum computation. Phys Rev Lett 91:187902
35. Zhu SL, Wang ZD, Zanardi P (2005) Geometric quantum computation and multiqubit entanglement with superconducting qubits inside a cavity. Phys Rev Lett 94:100502
36. Zhu SL, Zanardi P (2005) Geometric quantum gates that are robust against stochastic control errors. Phys Rev A 72:020301
37. Sjöqvist E, Tong DM, Andersson LM, Hessmo B, Johansson M, Singh K (2012) Non-adiabatic holonomic quantum computation. New J Phys 14:103035
38. Abdumalikov AA Jr, Fink JM, Juliusson K, Pechal M, Berger S, Wallraff A, Filipp S (2013) Experimental realization of non-Abelian non-adiabatic geometric gates. Nature 496:482–485
39. Feng G, Xu G, Long G (2013) Experimental realization of nonadiabatic holonomic quantum computation. Phys Rev Lett 110:190501
40. Ma Z, Xu J, Chen T, Zhang Y, Zheng W, Li S, Lan D, Xue ZY, Tan X, Yu Y (2023) Noncyclic nonadiabatic geometric quantum gates in a superconducting circuit. Phys Rev Appl 20:054047
41. Shen P, Liang Y, Chen T, Xue ZY (2023) Accelerated super-robust nonadiabatic holonomic quantum gates. Phys Rev A 108:032601
42. Berry MV (2009) Transitionless quantum driving. J Phys A, Math Theor 42:365303
43. Demirplak M, Rice SA (2003) Adiabatic population transfer with control fields. J Phys Chem A 107:9937–9945
44. Chen X, Lizuain I, Ruschhaupt A, Guéry-Odelin D, Muga JG (2010) Shortcut to adiabatic passage in two- and three-level atoms. Phys Rev Lett 105:123003
45. Huang BH, Kang YH, Chen YH, Wu QC, Song J, Xia Y (2017) Fast quantum state engineering via universal SU(2) transformation. Phys Rev A 96:022314
46. Chen YH, Shi ZC, Song J, Xia Y, Zheng SB (2017) Optimal shortcut approach based on an easily obtained intermediate Hamiltonian. Phys Rev A 95:062319
47. Lv QX, Liang ZT, Liu HZ, Liang JH, Liao KY, Du YX (2020) Noncyclic geometric quantum computation with shortcut to adiabaticity. Phys Rev A 101:022330
48. Liu YY, Sun Y, Fu Z, Xu P, Wang X, He XD, Wang J, Zhan MS (2021) Infidelity induced by ground-Rydberg decoherence of the control qubit in a two-qubit Rydberg-blockade gate. Phys Rev Appl 15:054020
49. Endres M, Bernien H, Keesling A, Levine H, Anschuetz ER, Krajenbrink A, Senko C, Vuletić V, Greiner M, Lukin MD (2016) Atom-by-atom assembly of defect-free one-dimensional cold atom arrays. Science 354:1024–1027
50. Hartung L, Seubert M, Welte S, Distante E, Rempe G (2024) A quantum-network register assembled with optical tweezers in an optical cavity. Science 385:179–183
51. Manetsch HJ, Nomura G, Bataille E, Leung KH, Lv XD, Endres M (2024) A tweezer array with 6100 highly coherent atomic qubits. arXiv:2403.12021
52. Schäfer VM, Ballance CJ, Thirumalai K, Stephenson LJ, Ballance TG, Steane AM, Lucas DM (2018) Fast quantum logic gates with trapped-ion qubits. Nature 555:75–78
53. Lu Y, Zhang SN, Zhang K, Chen WT, Shen Y, Zhang JL, Zhang JN, Kim K (2019) Global entangling gates on arbitrary ion qubits. Nature 572:363–367

Publisher's Note